Letter

Large anomalous Hall effect induced by weak ferromagnetism in the noncentrosymmetric antiferromagnet $CoNb_3S_6$

Hiroaki Tanaka,[1] Shota Okazaki,[2] Kenta Kuroda,[1,*] Ryo Noguchi,[1,3,4] Yosuke Arai,[1] Susumu Minami,[5] Shinichiro Ideta,[6,†] Kiyohisa Tanaka,[6] Donghui Lu,[7] Makoto Hashimoto,[7] Viktor Kandyba,[8] Mattia Cattelan,[8] Alexei Barinov,[8] Takayuki Muro,[9] Takao Sasagawa,[2,‡] and Takeshi Kondo[1,10,§]

[1]*Institute for Solid State Physics, The University of Tokyo, Kashiwa, Chiba 277-8581, Japan*
[2]*Materials and Structures Laboratory, Tokyo Institute of Technology, Yokohama, Kanagawa 226-8503, Japan*
[3]*Center for Correlated Electron Systems, Institute for Basic Science, Seoul 08826, Republic of Korea*
[4]*Department of Physics and Astronomy, Seoul National University, Seoul 08826, Republic of Korea*
[5]*Department of Physics, The University of Tokyo, Bunkyo-ku, Tokyo 113-0033, Japan*
[6]*UVSOR Facility, Institute for Molecular Science, Okazaki, Aichi 444-8585, Japan*
[7]*Stanford Synchrotron Radiation Lightsource, SLAC National Accelerator Laboratory, Menlo Park, California 94025, USA*
[8]*Elettra Sincrotrone Trieste, 34149 Basovizza, Trieste, Italy*
[9]*Japan Synchrotron Radiation Research Institute (JASRI), Sayo, Hyogo 679-5198, Japan*
[10]*Trans-scale Quantum Science Institute, The University of Tokyo, Bunkyo-ku, Tokyo 113-0033, Japan*

(Received 22 June 2021; revised 26 December 2021; accepted 17 February 2022; published 4 March 2022)

We study the mechanism of the exceptionally large anomalous Hall effect (AHE) in the noncentrosymmetric antiferromagnet $CoNb_3S_6$ by angle-resolved photoemission spectroscopy (ARPES) and magnetotransport measurements. From ARPES measurements of $CoNb_3S_6$ and its family compounds ($FeNb_3S_6$ and $NiNb_3S_6$), we find a band dispersion unique to the Co intercalation existing near the Fermi level. We further demonstrate that a slight deficiency of sulfur in $CoNb_3S_6$ eliminates the ferromagnetism and the AHE simultaneously while hardly changing the band structure, indicating that the weak ferromagnetism is responsible for the emergence of the large AHE. Based on our results, we propose Weyl points near the Fermi level to cause the large AHE.

DOI: 10.1103/PhysRevB.105.L121102

Transition metal dichalcogenides MX_2 (M: transition metal, X: chalcogen) exhibit various types of layered structures [1] and have gained attention as a platform to investigate enriched properties, such as superconductivity [2], charge density wave states [3], and band topology [4]. In these, both antiferromagnetism and ferromagnetism can be induced by intercalation of 3d magnetic elements [5,6]. Among these materials, great interest has been recently given to the noncentrosymmetric antiferromagnet $CoNb_3S_6$ [7], in which Co ions intercalated into $2H$-NbS_2 break the inversion symmetry [Fig. 1(a)]. The neutron scattering measurements revealed the collinear antiferromagnetic structure along the in-plane direction (Refs. [8,9] and Supplemental Material Fig. S1(a) [10]), which keeps the time-reversal symmetry.

Recently, weak ferromagnetism along the out-of-plane direction and large anomalous Hall effect (AHE) have been observed in $CoNb_3S_6$ [11]; interestingly, the anomalous Hall response is exceptionally large compared to the small ferromagnetic moment. When the intrinsic AHE [12,13] derived from the Berry curvature [14] is considered, the Hall resistivity can be decomposed as $\rho_{xy} = R_0\mu_0 H + R_s\mu_0 m$ [15]: here H and m are the magnetic field and magnetic moment density, whereas R_0 and R_s are coefficients for the ordinal Hall effect and AHE, respectively. R_s can be at most hundreds of times larger than R_0 (Refs. [16–21] and Supplemental Material Note 1 in [10]). For $CoNb_3S_6$, the ratio of R_s and R_0 is reported to be 5.9×10^4, much larger than usual cases. The relation between the weak ferromagnetism and the large AHE has been unclear. This issue has been all the more controversial because noncollinear antiferromagnetic structures [11,22] and emergent time-reversal symmetry breaking (Ref. [23] and Note 2 in [10]) have been proposed as alternative origins of the large AHE rather than the weak ferromagnetism.

In this Letter we used various techniques of angle-resolved photoemission spectroscopy (ARPES) with a wide range of photon energies from vacuum ultraviolet (VUV) light and soft x ray (SX) to study the electronic structure of $CoNb_3S_6$, and compared it with those of series materials NbS_2, $FeNb_3S_6$, $NiNb_3S_6$, and $CoNb_3S_{6-x}$. Our measurements unveil two unique properties of $CoNb_3S_6$. First, there is a specific band dispersion due to the Co intercalation, located very close to the Fermi level. Second, comparing magnetotransport properties, we revealed that the weak ferromagnetism and AHE observed in $CoNb_3S_6$ simultaneously disappeared in

*Present address: Graduate School of Advanced Science and Engineering, Hiroshima University, Higashi-hiroshima, Hiroshima 739-8526, Japan; kuroken224@hiroshima-u.ac.jp
†Present address: Hiroshima Synchrotron Radiation Center, Hiroshima University, Higashi-hiroshima, Hiroshima 739-0046, Japan.
‡sasagawa@msl.titech.ac.jp
§kondo1215@issp.u-tokyo.ac.jp

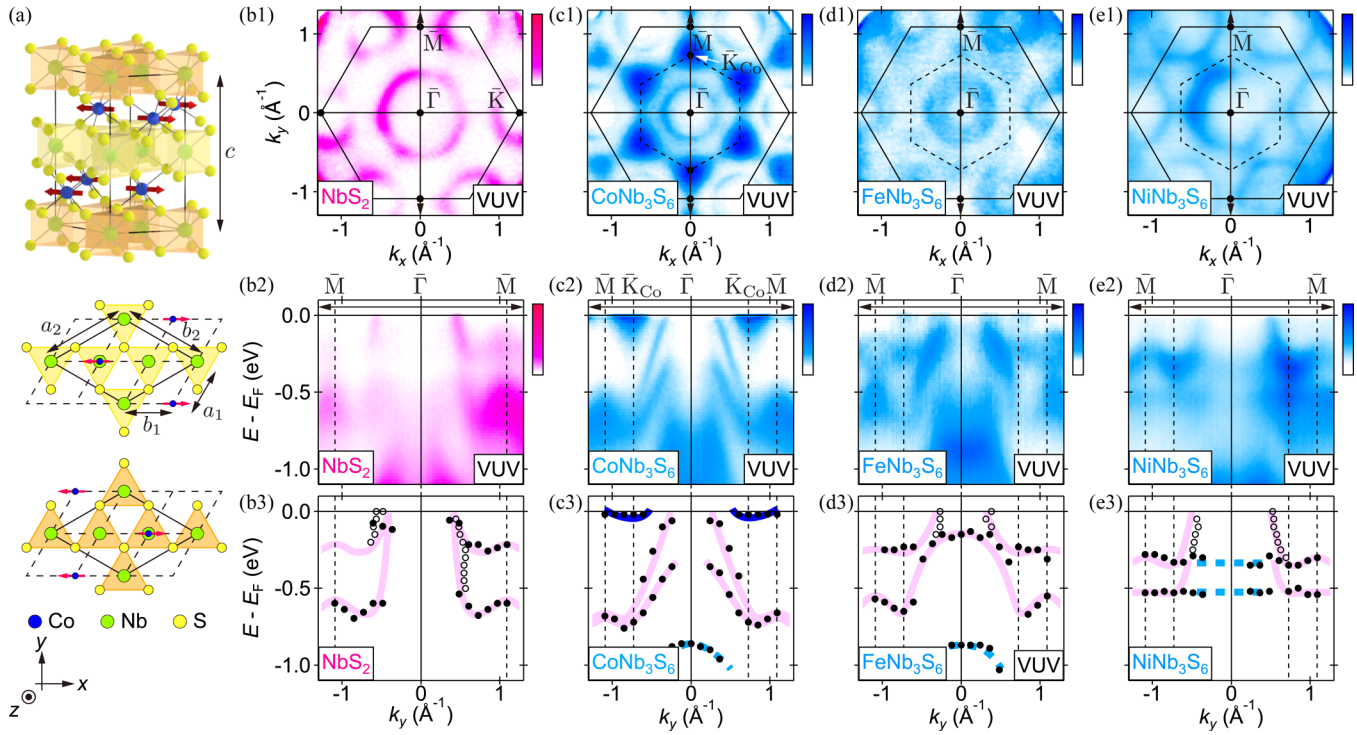

FIG. 1. Crystal structure and band dispersion of $CoNb_3S_6$ obtained by VUV-ARPES ($h\nu = 120$ eV). (a) Crystal structure of $CoNb_3S_6$. Two NbS_2 layers of different orientations are represented by orange and yellow. In the bottom panels, the crystallographic unit cells of NbS_2 and $CoNb_3S_6$ are represented by the dashed and solid rhomboids respectively. The red arrows represent antiferromagnetic moments of Co atoms. (b1) and (c1) Fermi surfaces of NbS_2 and $CoNb_3S_6$. (b2) and (c2) Band dispersions of NbS_2 and $CoNb_3S_6$ along the k_y direction [vertical arrows in (b1) and (c1)]. (b3) and (c3) Schematics of the band dispersions of NbS_2 and $CoNb_3S_6$. The black filled and open dots represent peak positions extracted from energy and momentum distribution curves (Figs. S7 and S8 [10]), respectively. Band dispersions originating from NbS_2 are drawn by pink and additional dispersions in (c3) are marked by blue or light blue. (d1)–(e3) Fermi surfaces and band dispersions of $FeNb_3S_6$ and $NiNb_3S_6$. In the Fermi surface maps, the solid and dashed hexagons correspond to the Brillouin zones of NbS_2 and MNb_3S_6 respectively.

$CoNb_3S_{6-x}$ with a sulfur deficiency, providing experimental evidence that the weak ferromagnetism is responsible for the emergence of the AHE. Focusing on the noncentrosymmetric nature of $CoNb_3S_6$, we propose that it enhances the AHE even under weak ferromagnetism because the broken time-reversal and inversion symmetries lead to Weyl points near the Fermi level originating from Kramers-Weyl nodes [24].

Single crystals of 2*H*-NbS_2, MNb_3S_6 (M = Fe, Co, Ni), and $CoNb_3S_{6-x}$ were grown by the chemical vapor transport method from polycrystals with iodine as the transport agent (see Note 3 in [10] for details). VUV-ARPES measurements were performed at BL5U of UVSOR and BL5-2 of SSRL, nano-VUV-ARPES was at Spectromicroscopy-3.2L beamline of Elettra Sincrotrone Trieste [25], and SX-ARPES was at BL25SU of SPring-8 [26,27] (see Note 4 in [10] for details). The measurement temperature was kept lower than 20 K in most measurements, other than temperature dependence (up to 200 K) and nano-VUV-ARPES measurements (30 K due to the machine limitation). In *ab initio* calculations based on the density functional theory (DFT) without spin, we used QUANTUM ESPRESSO code [28,29] and ultrasoft pseudopotentials [30,31]. Wannier90 [32] was also used to obtain the maximally localized Wannier functions.

We compare Fermi surface maps [Figs. 1(b1)–1(e1)] and band dispersions [Figs. 1(b2)–1(e2)] of $CoNb_3S_6$ and its series materials obtained by VUV-ARPES. NbS_2 has two Fermi pockets around the $\bar{\Gamma}$ and $\bar{K}$ points [Fig. 1(b1)]. The pocket around the $\bar{\Gamma}$ point is hole type containing two bands, drawn by the pink curves in the schematic [Fig. 1(b3)] (see Fig. S4(b) [10] center panel for the pocket around the $\bar{K}$ point). We found that the hole pocket around the $\bar{\Gamma}$ point became smaller in $CoNb_3S_6$ [Fig. 1(c1)]. This change can be observed as a band shift in the dispersion map [pink curves in Figs. 1(b3) and 1(c3)], which is consistent with our XPS measurements (Note 5 in [10]) and other intercalated materials [33,34].

Furthermore, we observed some additional bands in VUV-ARPES measurements of $CoNb_3S_6$ as illustrated by the blue and light blue curves in Fig. 1(c3). Among them, the tiny electron pockets at the corners of the Brillouin zone [blue curves in Fig. 1(c3)] are the most intriguing, because they can contribute to the AHE. While $FeNb_3S_6$ and $NiNb_3S_6$ also have additional occupied states (light blue dashed curves in Figs. 1(d3) and 1(e3); see Note 9 in [10] for the details of these states), these two materials have similar electronic structure as NbS_2 without the intercalation at the Fermi level. Although there seems to be intensity modulation near the Fermi level,

especially in $FeNb_3S_6$ [Figs. 1(d1) and 1(d2)], energy distribution curves of them [Figs. S7(c) and S7(d) [10]] have only small peaks. While they may indicate the existence of additional electronic states above the Fermi level, the additional band dispersion crossing the Fermi level is unique to the Co intercalation.

The additional electron pockets in $CoNb_3S_6$ originate from the bulk electronic structure and are dominated by Co atoms. SX-ARPES measurements of $CoNb_3S_6$ also captured these additional bands (Figs. S5(b) and S5(c) [10]) and k_z dependence of them (Fig. S5(d) [10]). Since SX-ARPES is bulk sensitive [35] and does not capture surface states such as topological Fermi arcs [36], these results show the bulk origin of these bands. For the second point, such dispersions do not exist in NbS_2 even if we considered unoccupied states calculated for NbS_2 [37], so this additional dispersion seems to come from Co atoms. This interpretation about the unique band was validated by surface-selective measurements using nanofocused light (Note 10 in [10]) and the intensity enhancement near the Fermi level at the energy on Co resonance (Figs. S5(f) and S5(g) [10]); the suppressed spectral intensities of this band at elevated temperatures also may be due to the disordered magnetic structure of Co atoms above T_N (Note 8 in [10]). We note that we carefully chose measurement positions in VUV-ARPES measurements (Fig. 1) to reduce the effect of termination-surface dependence (Note 11 in [10]).

Next we argue the effect of the broken inversion symmetry on wave functions in $CoNb_3S_6$, originating from the *AB* stacking of the original material 2*H*-NbS_2 (see Note 12 in [10] for details). Since the inversion operation exchanges *A* and *B* layers of 2*H*-NbS_2 [orange and yellow layers in Fig. 1(a)], we can consider the difference of wave functions on *A* and *B* layers as the strength of the noncentrosymmetric property for those in $CoNb_3S_6$. We claim that we can evaluate it from the ARPES spectrum intensities along the k_z direction; we focus on $4\pi/c$-periodic k_z dispersion, reported in ARPES measurements of *AB*-stacked materials [38,39]. First, we consider the k_z dispersions of one-layered (*AA*) and two-layered (*AB*) materials; the k_z dispersions contain one and two bands, respectively [Figs. 2(a) and 2(c)]. On the other hand, in a quasi-two-layered (AA') structure [Fig. 2(b)], where wave functions on two layers are only slightly different, the ARPES spectrum is expected to change from Fig. 2(a) only slightly, and therefore the spectrum intensities of two bands can be completely different [Fig. 2(b) bottom panel]. In general, the weak spectrum is experimentally undetectable, and the resulting $4\pi/c$ periodicity of the k_z dispersion is observed in most *AB*-stacked materials [38,39]. The one-dimensional tight-binding model with two orbitals (Ref. [40] and Note 13 in [10]) can discuss this argument more quantitatively.

Following the above argument, we performed bulk-sensitive SX-ARPES of NbS_2 and investigated the k_z dispersion [Fig. 2(d)]. The dispersion around $E - E_F = -2$ eV, highlighted by light blue, is one of the paired dispersions represented in the DFT calculations. This situation is the case where these two wave functions form a quasi-two-layered structure [Fig. 2(b)], similarly to previous research of *AB*-stacked materials [38,39]. On the other hand, two dispersions highlighted by blue form a pair, as confirmed by the inverted M-shaped bands along the k_y direction [Fig. 2(f)], which is

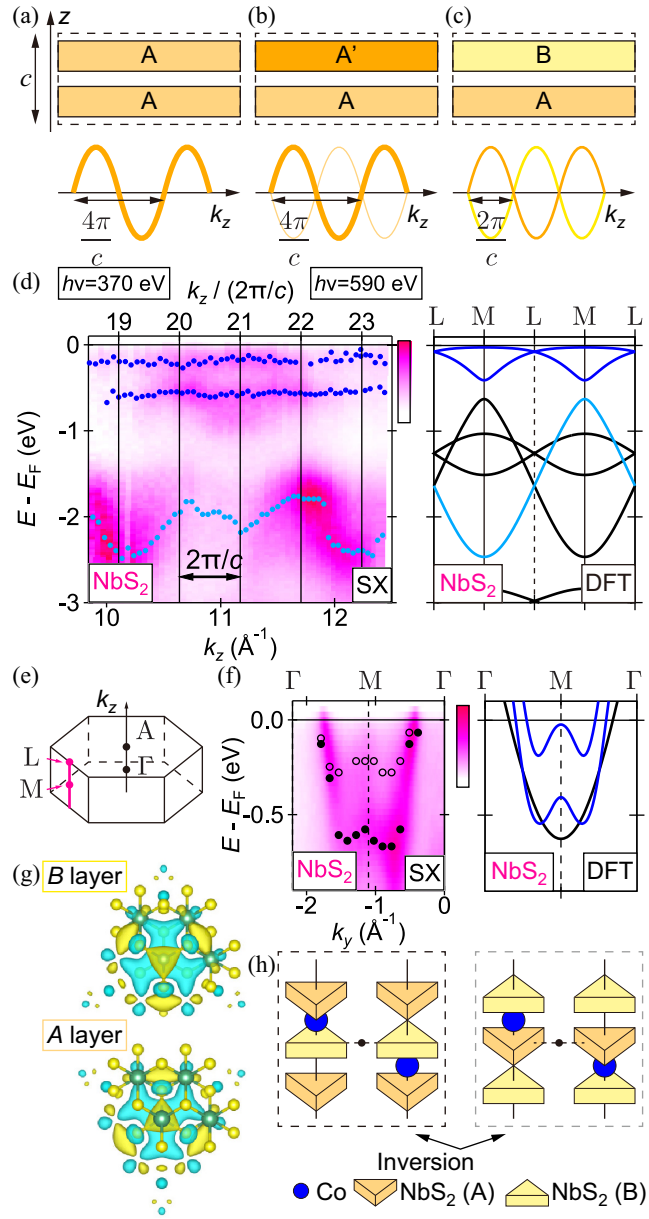

FIG. 2. Evaluation of the broken inversion symmetry in $CoNb_3S_6$ by the k_z dispersion of 2*H*-NbS_2. (a)–(c) Schematics of layered materials and estimated ARPES spectra along the k_z direction. (d) k_z dispersions of NbS_2 along the *M*-*L* path by SX-ARPES and DFT calculations. In the left panel, peak positions extracted from energy distribution curves (Fig. S15(a) [10]) are shown by the blue and light blue points. In the right panel, band dispersions corresponding to those observed by SX-ARPES are highlighted by the same colors. (e) Brillouin zone of NbS_2. (f) Band dispersions of SX-ARPES ($h\nu = 525$ eV) and DFT calculations along the k_y direction. Blue curves in the right panel correspond to those in (d). Filled and open circles in the left panel represent peak positions extracted from energy distribution curves (EDCs) [Figs. S14(b) and S14(c) [10]], while the open circles are those determined from EDC spectra in $k_y > 0$ region and symmetrized with respect to the Γ point. (g) Maximally localized Wannier functions of two bands highlighted by blue in (d) and (f). (h) Schematic of the electronic structure near the Fermi level. Left and right schematics are exchanged by the inversion for the black point, which keeps Co atoms unchanged.

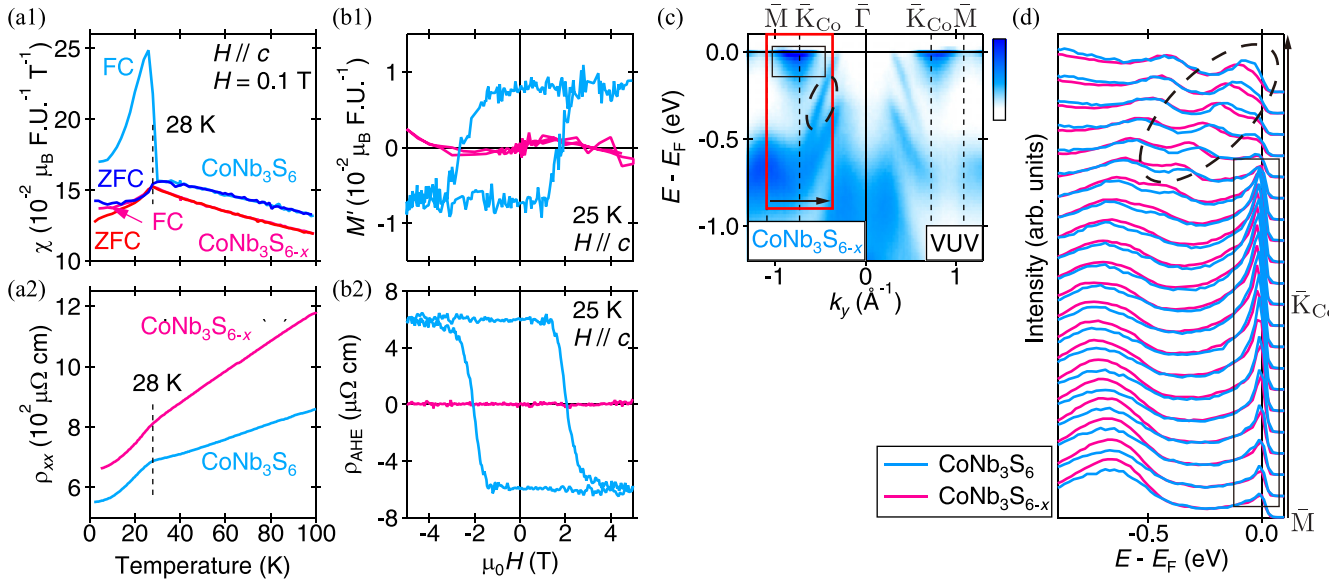

FIG. 3. Magnetic and magnetotransport properties of $CoNb_3S_6$. (a1) Magnetic susceptibility χ of $CoNb_3S_6$ (light blue and blue) and $CoNb_3S_{6-x}$ (pink and red), obtained by field-cooled (FC) and zero-field-cooled (ZFC) processes. (a2) Temperature dependence of the longitudinal resistivity ρ_{xx} in $CoNb_3S_6$ (light blue) and $CoNb_3S_{6-x}$ (pink). (b1) Out-of-plane ferromagnetic moment extracted from M-H curves like Fig. S16(b) [10]. (b2) Anomalous Hall resistivity ρ_{AHE} extracted from ρ_{xy}-H curves like Fig. S16(c) [10]. (c) Band dispersion of $CoNb_3S_{6-x}$ along the k_y direction taken by the 120 eV VUV light. (d) Energy distribution curves of $CoNb_3S_6$ and $CoNb_3S_{6-x}$ in the red rectangular area in (c). The dashed ovals and solid rectangles in (c) and (d) correspond to each other.

the case of Fig. 2(c). This situation is consistent with the maximally localized Wannier functions of these bands, having triangular shapes and resulting in small overlap with each other [Fig. 2(g)]. Therefore, in $CoNb_3S_6$ these dispersions contribute to the substantially broken inversion symmetry of the electronic structure near the Fermi level [Fig. 2(h)].

As a minor difference of SX-ARPES measurements and DFT calculations, we did not observe the band degenerations at L points. Since they are associated with 2_1 screw rotational symmetry [41,42], this result can be because, while SX-ARPES is bulk sensitive, it can detect the electronic structure in a few layers near the surface, where the screw rotational symmetry is incomplete. Although this observation does not affect much our discussion of the broken inversion symmetry, we need further experiments and calculations to explain it in more detail.

To better understand the mechanism of the large AHE in $CoNb_3S_6$, we prepared $CoNb_3S_{6-x}$ with a sulfur deficiency, and compared their electronic structures and magnetotransport properties. We observed kinks at $T_N \simeq 28$ K in the magnetic susceptibility and longitudinal resistivity measurements of not only $CoNb_3S_6$ [11,22] but also $CoNb_3S_{6-x}$ [Figs. 3(a1) and 3(a2)]. However, only $CoNb_3S_6$ exhibited the abrupt jump of the magnetic susceptibility at T_N, associated with out-of-plane ferromagnetic moment. This difference is also observed by magnetic-field dependence measurements of the out-of-plane ferromagnetic moment [Fig. 3(b1)]. For $CoNb_3S_6$, the ferromagnetic moment and AHE showed hysteresis curves with the same coercive magnetic field [light blue curves in Figs. 3(b1) and 3(b2)], as previously reported [11]. Although the ferromagnetic moment is larger than previous research, the ratio of R_s and R_0 is still exceptionally large (Note 1 in [10]). On the other hand, such hysteresis curves completely vanished in $CoNb_3S_{6-x}$ [pink curves in Figs. 3(b1) and 3(b2)].

In contrast to the clear difference in the magnetotransport properties, VUV-ARPES measurements of $CoNb_3S_{6-x}$ revealed that the band dispersion is almost the same as that of $CoNb_3S_6$ [Figs. 1(c2) and 3(c)], as well as the unique band near the Fermi level. As a clear difference, we only found band shift as small as 50 meV in the area represented by the dashed oval in Fig. 3(d) (see Fig. S17(b) [10] for $k_y > 0$), which corresponds to the band dispersion originating from NbS_2 layers. While this variation can be explained by electron doping due to the vacancy of electronegative sulfur atoms, negligible change of the unique band originating from Co atoms, highlighted by the solid rectangle in Fig. 3(d), show that Co atoms are more weakly affected by the electron doping than NbS_2 layers. Such a slight difference cannot account for the complete disappearance of the AHE, so we conclude that the weak ferromagnetism is responsible for the emergence of the AHE in $CoNb_3S_6$ (see Note 15 in [10] for other magnetic and magnetotransport properties).

We propose that Weyl points near the Fermi level may cause the large AHE even under the weak ferromagnetism. Without the ferromagnetic moment, this system should have Kramers-Weyl nodes, which are Weyl points at time-reversal invariant momenta (TRIMs) as a result of the noncentrosymmetric crystal structure [24]. The Kramers-Weyl node at the M_{Co} point for the unique band is expected to be very close to the Fermi level [Fig. 4(a) center panel and 4(b)]; on the contrary, $FeNb_3S_6$ and $NiNb_3S_6$ have band dispersions of NbS_2 and occupied Fe/Ni bands in Fig. 4(a). Although these occupied states also might have Kramers-Weyl nodes, they are unrelated to magnetotransport properties such as the AHE.

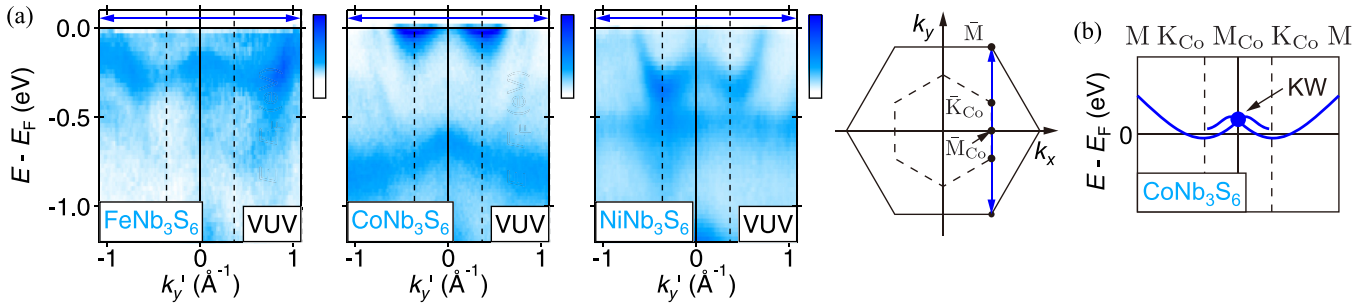

FIG. 4. Possibility of Kramers-Weyl nodes near the Fermi level in $CoNb_3S_6$. (a) Band dispersions of MNb_3S_6 (M = Fe, Co, Ni) along the blue arrow in the right schematic of the Brillouin zones. (b) Schematic of band dispersions near the Fermi level for $CoNb_3S_6$. The Kramers-Weyl node is marked by the blue circle and labeled as "KW."

With broken time-reversal symmetry by the ferromagnetic moment, such a system emerges nonzero anomalous Hall conductance (Note 17 in [10]). In this case, Weyl points should exist near the Fermi level, so the resultant anomalous Hall conductance is expected to be large even if the ferromagnetic moment is small, as discussed in other magnetic Weyl semimetals with the inversion symmetry [19,43–45]. Since the inversion symmetry is evaluated to be substantially broken by analyzing the k_z dispersion (Fig. 2), the spin splitting of the noncentrosymmetric system should not be ignored, which is another preferable condition for the emergence of the large AHE. These Weyl points associated with Kramers-Weyl nodes can be possible only in materials with both the broken time-reversal and inversion symmetries. Since most magnetic Weyl semimetals are centrosymmetric such as Mn_3Sn [43,44] and $Co_3Sn_2S_2$ [19,45], the noncentrosymmetric $CoNb_3S_6$ could be a new type of magnetic Weyl semimetals showing the large AHE.

In conclusion, we experimentally studied the electronic structure and the large AHE of $CoNb_3S_6$ via the comparison with its series materials. VUV- and SX-ARPES measurements revealed the unique band dispersion near the Fermi level derived from the Co intercalation. SX-ARPES spectra of NbS_2 along the k_z direction indicated that the electronic structure of $CoNb_3S_6$ near the Fermi level substantially breaks the inversion symmetry. While the possibility of a noncollinear magnetic structure has been proposed to explain the large AHE [11,22], our magnetic and magnetotransport measurements of $CoNb_3S_6$ revealed that the weak ferromagnetism is responsible for the emergence of the AHE. Based on our results, we propose the existence of Weyl points near the Fermi level, associated with the Kramers-Weyl node system in noncentrosymmetric crystal structures [24], which could cause the large AHE even if the ferromagnetism is weak.

We thank Y. Ishida for supporting the analysis of ARPES data [57], and M. Hirayama, T. Nomoto, and R. Arita for fruitful discussions. R.N. was supported by the Institute for Basic Science in Korea (Grant No. IBS-R009-G2). This work is also supported by Grants-in-Aid for JSPS Fellows (Grant No. JP21J20657), Grants-in-Aid for Scientific Research(B) (Grant No. JP19H02683), Grants-in-Aid for Scientific Research(A) (Grants No. JP19H00651, No. JP20H00337, No. JP21H04439, and No. JP21H04652), the Murata Science Foundation, Photon and Quantum Basic Research Coordinated Development Program from MEXT, CREST project (JPMJCR16F2) from JST, MEXT Q-LEAP (Grant No. JPMXS0118068681), and by MEXT under the Program for Promoting Researches on the Supercomputer Fugaku (Basic Science for Emergence and Functionality in Quantum Matter Innovative Strongly Correlated Electron Science by Integration of Fugaku and Frontier Experiments) (Project No. hp200132). Use of the Stanford Synchrotron Radiation Lightsource, SLAC National Accelerator Laboratory, is supported by the U.S. Department of Energy, Office of Science, Office of Basic Energy Sciences under Contract No. DE-AC02-76SF00515. The synchrotron radiation experiments were performed with the approval of UVSOR (Proposals No. 20-757 and No. 20-842), Elettra Sincrotrone Trieste (Proposal No. 20200395), and JASRI (Proposal No. 2020A1181).

H.T. and S.O. contributed equally to this work.

[1] A. V. Kolobov and J. Tominaga, *Two-Dimensional Transition-Metal Dichalcogenides* (Springer, Berlin, 2016).

[2] T. Yokoya, T. Kiss, A. Chainani, S. Shin, M. Nohara, and H. Takagi, Science **294**, 2518 (2001).

[3] J. Wilson, F. D. Salvo, and S. Mahajan, Adv. Phys. **24**, 117 (1975).

[4] A. A. Soluyanov, D. Gresch, Z. Wang, Q. Wu, M. Troyer, X. Dai, and B. A. Bernevig, Nature (London) **527**, 495 (2015).

[5] R. H. Friend, A. R. Beal, and A. D. Yoffe, Philos. Mag.: J. Theor. Exper. Appl. Phys. **35**, 1269 (1977).

[6] S. S. P. Parkin and R. H. Friend, Philos. Mag. B **41**, 65 (1980).

[7] In this report we use "noncentrosymmetric" instead of "chiral" in the meaning of the broken inversion symmetry, because they are different in some crystallographic contexts [58].

[8] S. S. P. Parkin, E. A. Marseglia, and P. J. Brown, J. Phys. C **16**, 2765 (1983).

[9] MAGNDATA data base: http://webbdcrista1.ehu.es/magndata/index.php.

[10] See Supplemental Material at http://link.aps.org/supplemental/10.1103/PhysRevB.105.L121102 for crystal characterization, additional ARPES data, DFT calculations, and which includes Refs. [46–56].

[11] N. J. Ghimire, A. S. Botana, J. S. Jiang, J. Zhang, Y.-S. Chen, and J. F. Mitchell, Nat. Commun. **9**, 3280 (2018).

[12] D. J. Thouless, M. Kohmoto, M. P. Nightingale, and M. den Nijs, Phys. Rev. Lett. **49**, 405 (1982).

[13] M. Onoda and N. Nagaosa, J. Phys. Soc. Jpn. **71**, 19 (2002).

[14] M. V. Berry, Proc. R. Soc. London Sect. A **392**, 45 (1984).

[15] N. Nagaosa, J. Sinova, S. Onoda, A. H. MacDonald, and N. P. Ong, Rev. Mod. Phys. **82**, 1539 (2010).

[16] E. M. Pugh, Phys. Rev. **36**, 1503 (1930).

[17] Q. Wang, S. Sun, X. Zhang, F. Pang, and H. Lei, Phys. Rev. B **94**, 075135 (2016).

[18] L. Ye, M. Kang, J. Liu, F. von Cube, C. R. Wicker, T. Suzuki, C. Jozwiak, A. Bostwick, E. Rotenberg, D. C. Bell, L. Fu, R. Comin, and J. G. Checkelsky, Nature (London) **555**, 638 (2018).

[19] E. Liu, Y. Sun, N. Kumar, L. Muechler, A. Sun, L. Jiao, S.-Y. Yang, D. Liu, A. Liang, Q. Xu, J. Kroder, V. Süß, H. Borrmann, C. Shekhar, Z. Wang, C. Xi, W. Wang, W. Schnelle, S. Wirth, Y. Chen *et al.*, Nat. Phys. **14**, 1125 (2018).

[20] J. Dijkstra, P. J. Zijlema, C. F. van Bruggen, C. Haas, and R. A. de Groot, J. Phys.: Condens. Matter **1**, 6363 (1989).

[21] J. G. Checkelsky, M. Lee, E. Morosan, R. J. Cava, and N. P. Ong, Phys. Rev. B **77**, 014433 (2008).

[22] G. Tenasini, E. Martino, N. Ubrig, N. J. Ghimire, H. Berger, O. Zaharko, F. Wu, J. F. Mitchell, I. Martin, L. Forró, and A. F. Morpurgo, Phys. Rev. Research **2**, 023051 (2020).

[23] L. Šmejkal, R. González-Hernández, T. Jungwirth, and J. Sinova, Sci. Adv. **6**, aaz8809 (2020).

[24] G. Chang, B. J. Wieder, F. Schindler, D. S. Sanchez, I. Belopolski, S.-M. Huang, B. Singh, D. Wu, T.-R. Chang, T. Neupert, S.-Y. Xu, H. Lin, and M. Z. Hasan, Nat. Mater. **17**, 978 (2018).

[25] P. Dudin, P. Lacovig, C. Fava, E. Nicolini, A. Bianco, G. Cautero, and A. Barinov, J. Synchrotron Radiat. **17**, 445 (2010).

[26] Y. Senba, H. Ohashi, Y. Kotani, T. Nakamura, T. Muro, T. Ohkochi, N. Tsuji, H. Kishimoto, T. Miura, M. Tanaka, M. Higashiyama, S. Takahashi, Y. Ishizawa, T. Matsushita, Y. Furukawa, T. Ohata, N. Nariyama, K. Takeshita, T. Kinoshita, A. Fujiwara *et al.*, AIP Conf. Proc. **1741**, 030044 (2016).

[27] T. Muro, Y. Senba, H. Ohashi, T. Ohkochi, T. Matsushita, T. Kinoshita, and S. Shin, J. Synchrotron Radiat. **28**, 1631 (2021).

[28] P. Giannozzi, S. Baroni, N. Bonini, M. Calandra, R. Car, C. Cavazzoni, D. Ceresoli, G. L. Chiarotti, M. Cococcioni, I. Dabo, A. D. Corso, S. de Gironcoli, S. Fabris, G. Fratesi, R. Gebauer, U. Gerstmann, C. Gougoussis, A. Kokalj, M. Lazzeri, L. Martin-Samos *et al.*, J. Phys.: Condens. Matter **21**, 395502 (2009).

[29] P. Giannozzi, O. Andreussi, T. Brumme, O. Bunau, M. B. Nardelli, M. Calandra, R. Car, C. Cavazzoni, D. Ceresoli, M. Cococcioni, N. Colonna, I. Carnimeo, A. D. Corso, S. de Gironcoli, P. Delugas, R. A. DiStasio, A. Ferretti, A. Floris, G. Fratesi, G. Fugallo *et al.*, J. Phys.: Condens. Matter **29**, 465901 (2017).

[30] A. M. Rappe, K. M. Rabe, E. Kaxiras, and J. D. Joannopoulos, Phys. Rev. B **41**, 1227 (1990).

[31] We used the pseudopotentials Nb.pbe-spn-rrkjus_psl.1.0.0.UPF and S.pbe-n-rrkjus_psl.1.0.0.UPF from the QUANTUM ESPRESSO pseudopotential data base: http://www.quantum-espresso.org/pseudopotentials.

[32] G. Pizzi, V. Vitale, R. Arita, S. Blügel, F. Freimuth, G. Géranton, M. Gibertini, D. Gresch, C. Johnson, T. Koretsune, J. Ibañez-Azpiroz, H. Lee, J.-M. Lihm, D. Marchand, A. Marrazzo, Y. Mokrousov, J. I. Mustafa, Y. Nohara, Y. Nomura, L. Paulatto *et al.*, J. Phys.: Condens. Matter **32**, 165902 (2020).

[33] C. Battaglia, H. Cercellier, L. Despont, C. Monney, M. Prester, H. Berger, L. Forró, M. G. Garnier, and P. Aebi, Eur. Phys. J. B **57**, 385 (2007).

[34] N. Sirica, S.-K. Mo, F. Bondino, I. Pis, S. Nappini, P. Vilmercati, J. Yi, Z. Gai, P. C. Snijders, P. K. Das, I. Vobornik, N. Ghimire, M. R. Koehler, L. Li, D. Sapkota, D. S. Parker, D. G. Mandrus, and N. Mannella, Phys. Rev. B **94**, 075141 (2016).

[35] V. Strocov, L. Lev, M. Kobayashi, C. Cancellieri, M.-A. Husanu, A. Chikina, N. Schröter, X. Wang, J. Krieger, and Z. Salman, J. Electron Spectrosc. Relat. Phenom. **236**, 1 (2019).

[36] S.-Y. Xu, I. Belopolski, N. Alidoust, M. Neupane, G. Bian, C. Zhang, R. Sankar, G. Chang, Z. Yuan, C.-C. Lee, S.-M. Huang, H. Zheng, J. Ma, D. S. Sanchez, B. Wang, A. Bansil, F. Chou, P. P. Shibayev, H. Lin, S. Jia *et al.*, Science **349**, 613 (2015).

[37] In this argument we used DFT calculations of NbS_2 to estimate the unoccupied states. Since the unoccupied bands are located above $E_F + 2$ eV as described in Fig. S12(e), these bands cannot appear even if the band shift at most 1 eV, which we evaluated by XPS measurements, is considered.

[38] D. Di Sante, P. K. Das, C. Bigi, Z. Ergönenc, N. Gürtler, J. A. Krieger, T. Schmitt, M. N. Ali, G. Rossi, R. Thomale, C. Franchini, S. Picozzi, J. Fujii, V. N. Strocov, G. Sangiovanni, I. Vobornik, R. J. Cava, and G. Panaccione, Phys. Rev. Lett. **119**, 026403 (2017).

[39] F. Matsui, H. Nishikawa, H. Daimon, M. Muntwiler, M. Takizawa, H. Namba, and T. Greber, Phys. Rev. B **97**, 045430 (2018).

[40] S. Moser, J. Electron Spectrosc. Relat. Phenom. **214**, 29 (2017).

[41] Q.-F. Liang, J. Zhou, R. Yu, Z. Wang, and H. Weng, Phys. Rev. B **93**, 085427 (2016).

[42] K. Funada, A. Yamakage, N. Yamashina, and H. Kageyama, J. Phys. Soc. Jpn. **88**, 044711 (2019).

[43] H. Yang, Y. Sun, Y. Zhang, W.-J. Shi, S. S. P. Parkin, and B. Yan, New J. Phys. **19**, 015008 (2017).

[44] K. Kuroda, T. Tomita, M.-T. Suzuki, C. Bareille, A. A. Nugroho, P. Goswami, M. Ochi, M. Ikhlas, M. Nakayama, S. Akebi, R. Noguchi, R. Ishii, N. Inami, K. Ono, H. Kumigashira, A. Varykhalov, T. Muro, T. Koretsune, R. Arita, S. Shin *et al.*, Nat. Mater. **16**, 1090 (2017).

[45] D. F. Liu, A. J. Liang, E. K. Liu, Q. N. Xu, Y. W. Li, C. Chen, D. Pei, W. J. Shi, S. K. Mo, P. Dudin, T. Kim, C. Cacho, G. Li, Y. Sun, L. X. Yang, Z. K. Liu, S. S. P. Parkin, C. Felser, and Y. L. Chen, Science **365**, 1282 (2019).

[46] Y. Saitoh, K. Kobayashi, A. Fujimori, Y. Yamamura, M. Koyano, T. Tsuji, and S. Katayama, J. Electron Spectrosc. Relat. Phenom. **144–147**, 829 (2005).

[47] P. V. C. Medeiros, S. Stafström, and J. Björk, Phys. Rev. B **89**, 041407(R) (2014).

[48] P. V. C. Medeiros, S. S. Tsirkin, S. Stafström, and J. Björk, Phys. Rev. B **91**, 041116(R) (2015).

[49] C.-C. Lee, Y. Yamada-Takamura, and T. Ozaki, J. Phys.: Condens. Matter **25**, 345501 (2013).

[50] T. Kondo, R. Khasanov, J. Karpinski, S. M. Kazakov, N. D. Zhigadlo, T. Ohta, H. M. Fretwell, A. D. Palczewski, J. D. Koll, J. Mesot, E. Rotenberg, H. Keller, and A. Kaminski, Phys. Rev. Lett. **98**, 157002 (2007).

[51] M. Kang, L. Ye, S. Fang, J.-S. You, A. Levitan, M. Han, J. I. Facio, C. Jozwiak, A. Bostwick, E. Rotenberg, M. K. Chan, R. D. McDonald, D. Graf, K. Kaznatcheev, E. Vescovo, D. C. Bell, E. Kaxiras, J. van den Brink, M. Richter, M. Prasad Ghimire *et al.*, Nat. Mater. **19**, 163 (2020).

[52] H. Iwasawa, N. B. M. Schröter, T. Masui, S. Tajima, T. K. Kim, and M. Hoesch, Phys. Rev. B **98**, 081112(R) (2018).

[53] H. Iwasawa, P. Dudin, K. Inui, T. Masui, T. K. Kim, C. Cacho, and M. Hoesch, Phys. Rev. B **99**, 140510(R) (2019).

[54] K. Nakayama, S. Souma, C. X. Trang, D. Takane, C. Chen, J. Avila, T. Takahashi, S. Sasaki, K. Segawa, M. C. Asensio, Y. Ando, and T. Sato, Nano Lett. **19**, 3737 (2019).

[55] L. Xu, Y. Mao, H. Wang, J. Li, Y. Chen, Y. Xia, Y. Li, D. Pei, J. Zhang, H. Zheng, K. Huang, C. Zhang, S. Cui, A. Liang, W. Xia, H. Su, S. Jung, C. Cacho, M. Wang, G. Li *et al.*, Sci. Bull. **65**, 2086 (2020).

[56] N. Sirica, P. Vilmercati, F. Bondino, I. Pis, S. Nappini, S.-K. Mo, A. V. Fedorov, P. K. Das, I. Vobornik, J. Fujii, L. Li, D. Sapkota, D. S. Parker, D. G. Mandrus, and N. Mannella, Commun. Phys. **3**, 65 (2020).

[57] Y. Ishida and S. Shin, Rev. Sci. Instrum. **89**, 043903 (2018).

[58] G. Burns and A. Glazer, *Space Groups for Solid State Scientists (Third Edition)* (Academic, Oxford, 2013).